10.1071/CH21129_AC

Australian Journal of Chemistry

Supplementary Material

Monometallic and Multimetallic Zinc Complexes of 2,7-Bis(2-pyridyl)-1,8-naphthyridine

Michael A. Stevens,[A] Peter D. Hall,[A] and Annie L. Colebatch[A,B]

[A]Research School of Chemistry, Australian National University, Canberra, ACT 2601, Australia.
[B]Corresponding author. Email: annie.colebatch@anu.edu.au

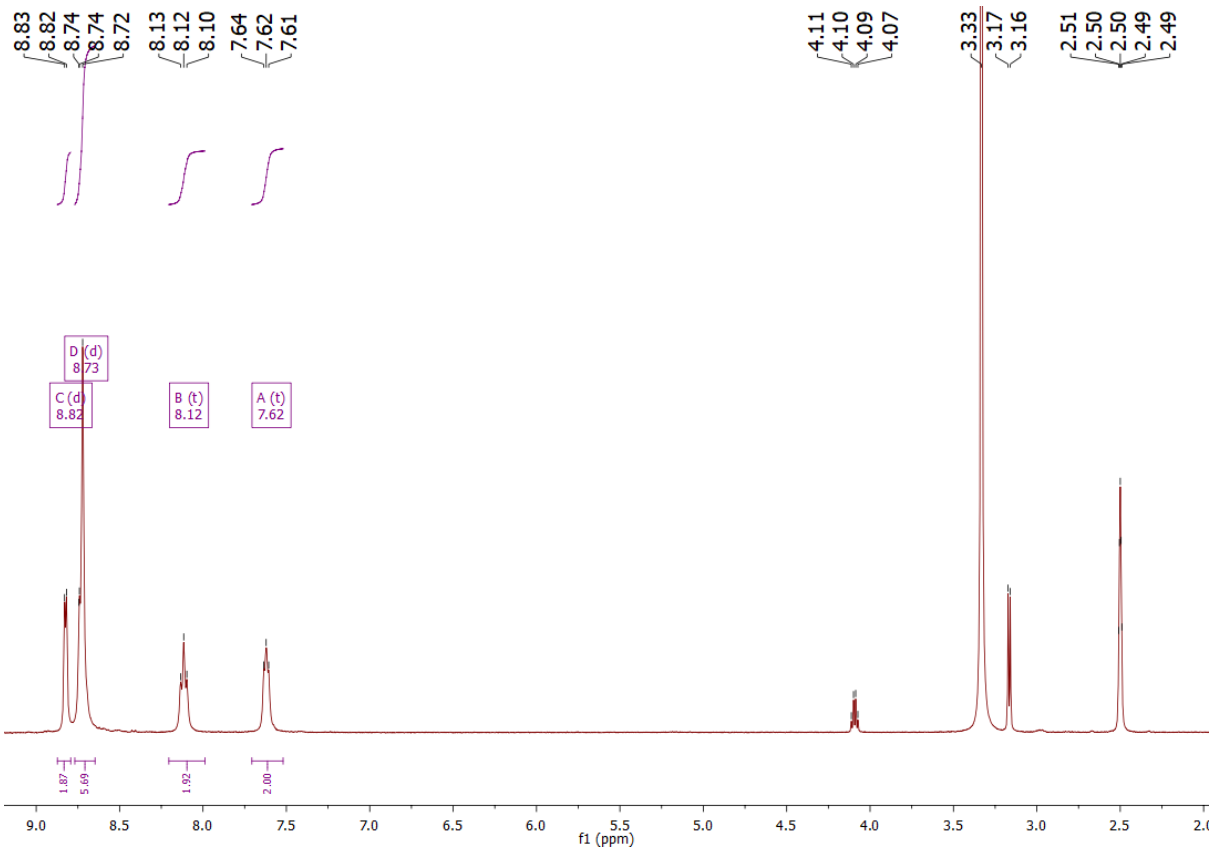

Figure S1: ^{1}H NMR spectrum of [Zn(BPNP)Cl$_2$] (**1**) in DMSO-*d*$_6$. A small quantity of residual methanol is present at 3.17 and 4.10 ppm.

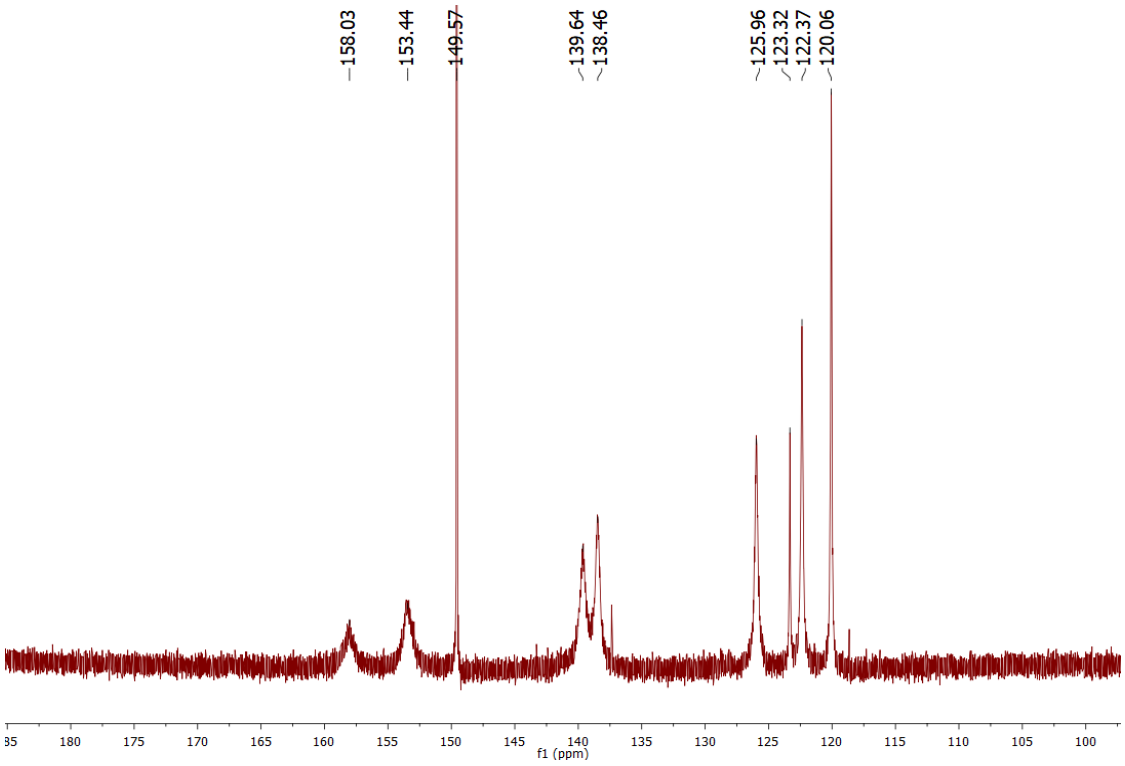

Figure S2: ^{13}C{^{1}H} NMR spectrum (aromatic region) of [Zn(BPNP)Cl$_2$] (**1**) in DMSO-*d*$_6$.

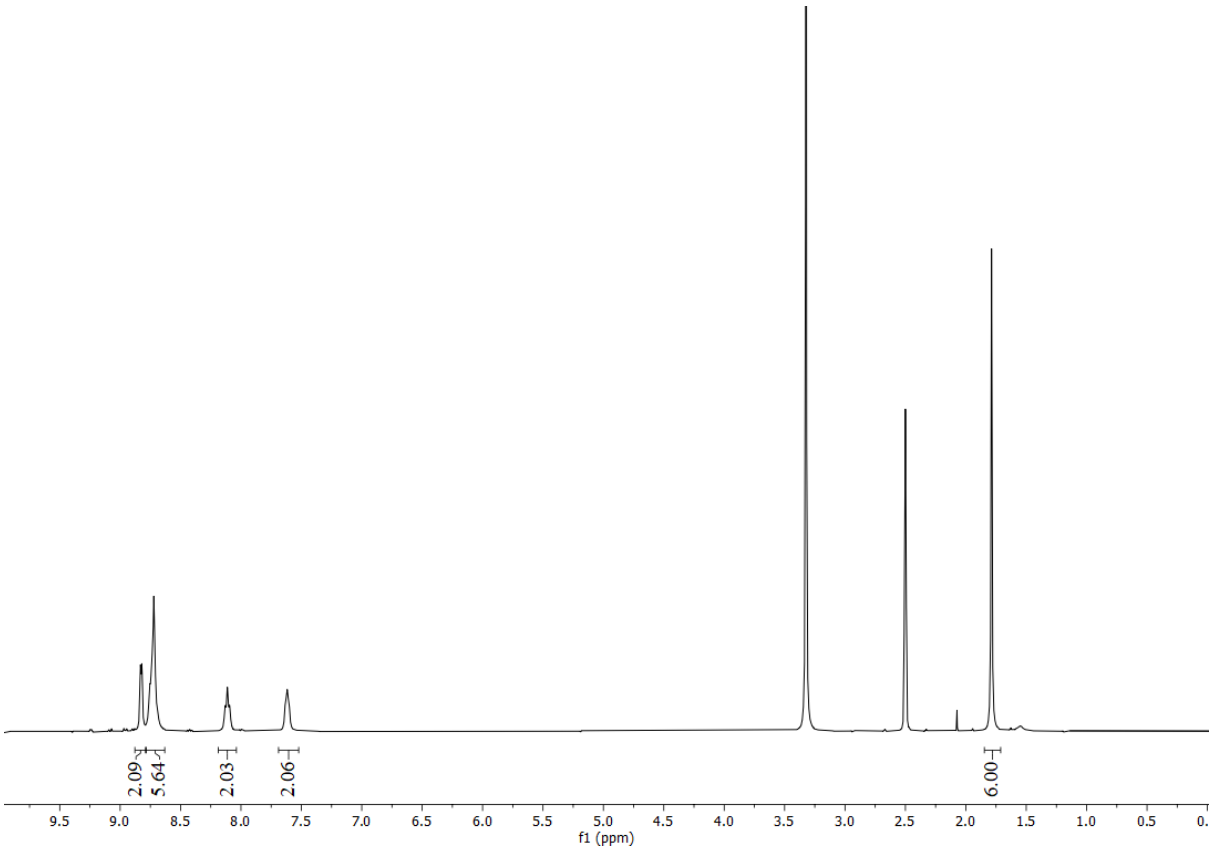

Figure S3: ^{1}H NMR spectrum of [Zn(BPNP)(OAc)$_2$] (**2**) in DMSO-*d*$_6$.

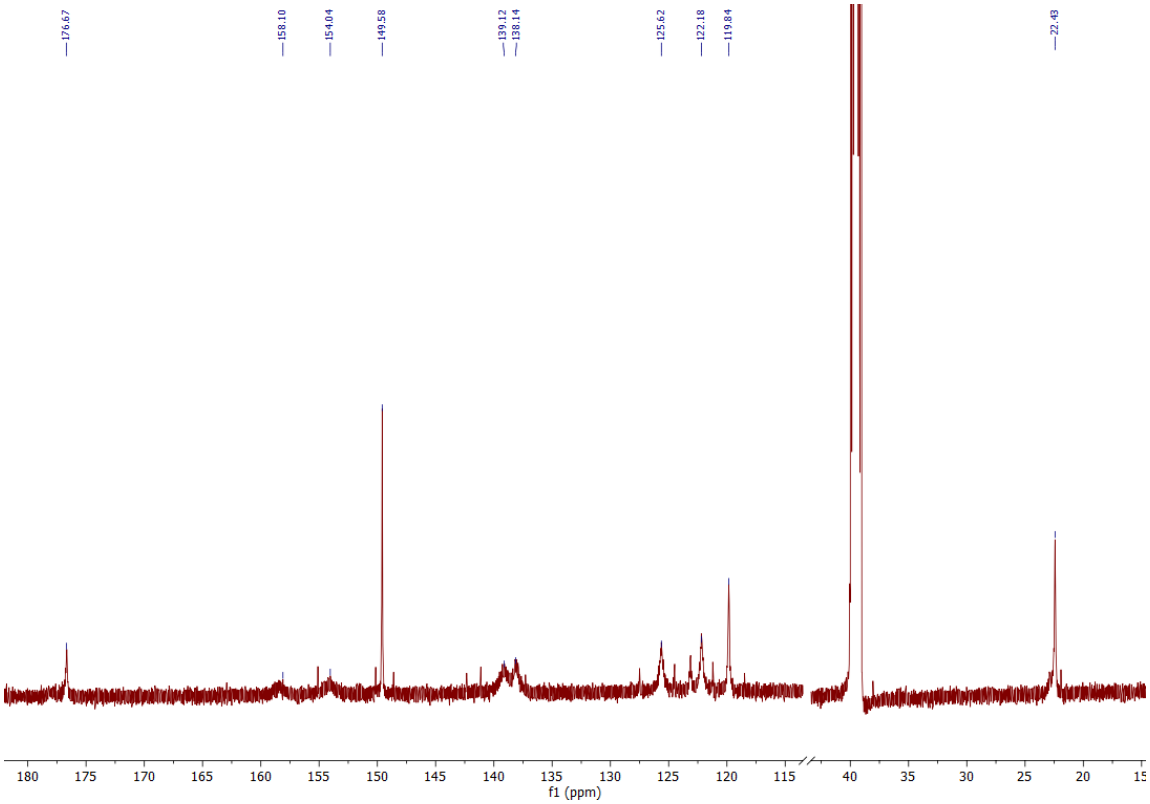

Figure S4: ^{13}C{^{1}H} NMR spectrum of [Zn(BPNP)(OAc)$_2$] (**2**) in DMSO-*d*$_6$.

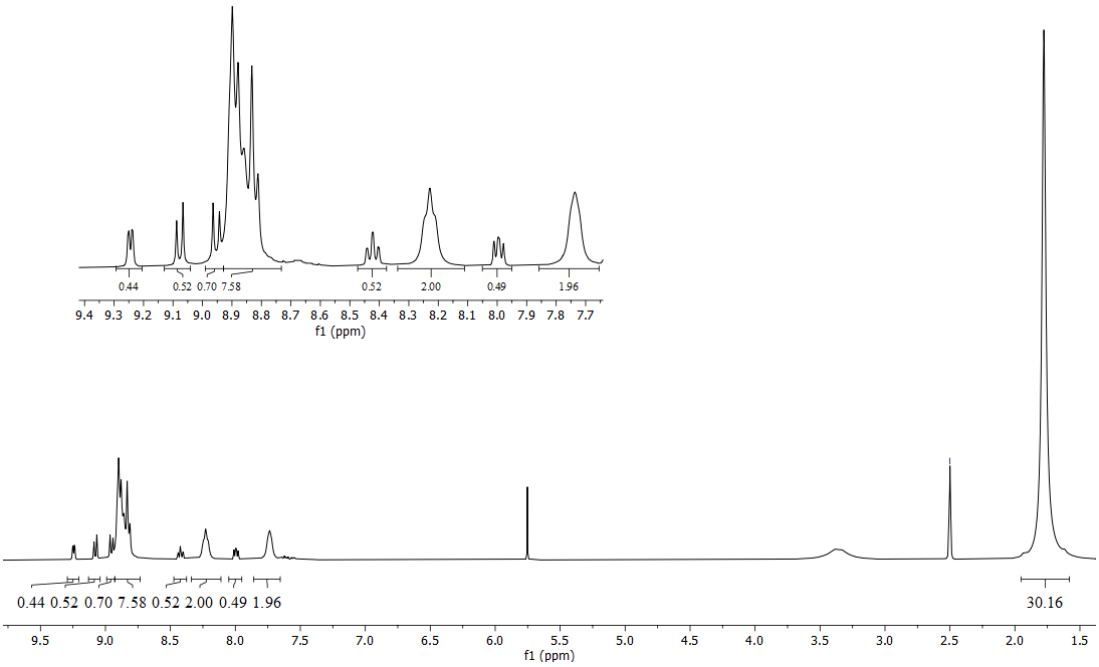

Figure S5: ^{1}H NMR spectrum of a mixture of [Zn_3(μ_2-BPNP)(μ_2-OAc)$_3$(OAc)$_2$(μ_3-OH)] (**3**) and [Zn(BPNP)(OAc)$_2$] (**2**) in DMSO-*d*$_6$. A small quantity of residual DCM is present from the ligand synthesis.

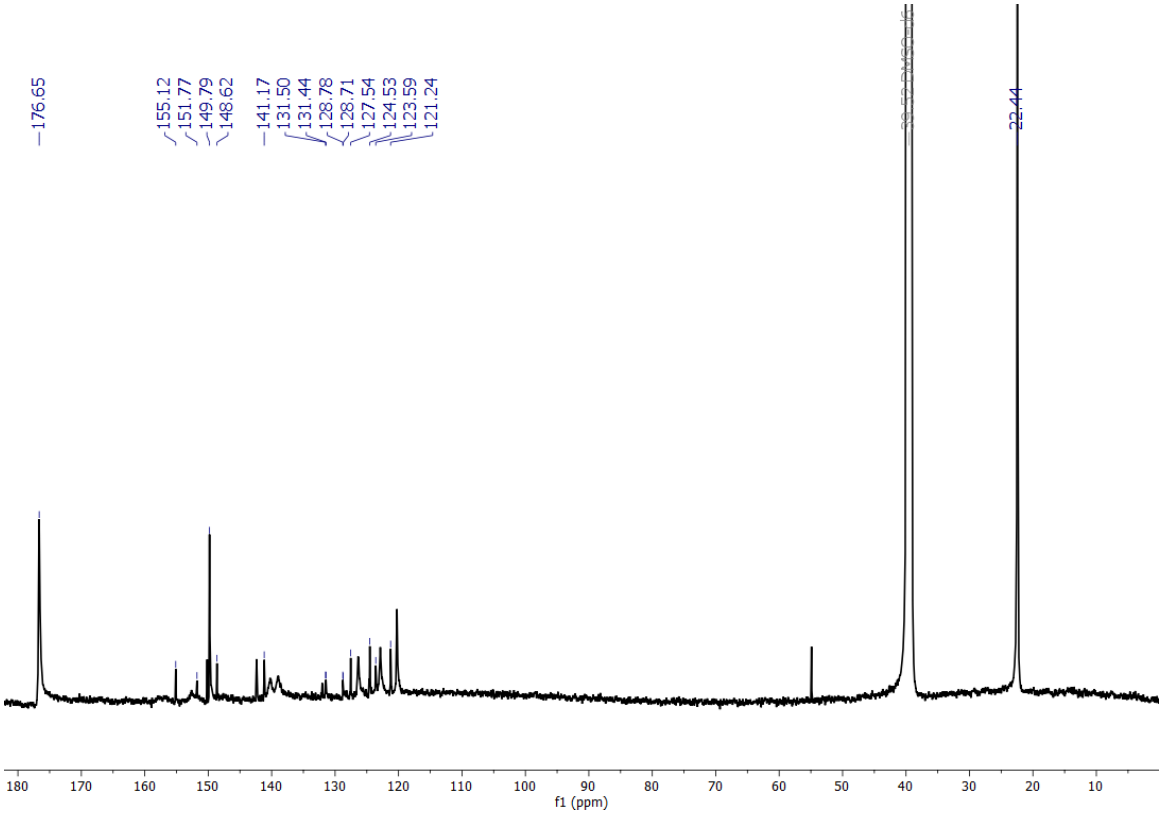

Figure S6: ^{13}C{^{1}H} NMR spectrum of a mixture of [Zn_3(μ_2-BPNP)(μ_2-OAc)$_3$(OAc)$_2$(μ_3-OH)] (**3**) and [Zn(BPNP)(OAc)$_2$] (**2**) in DMSO-*d*$_6$.

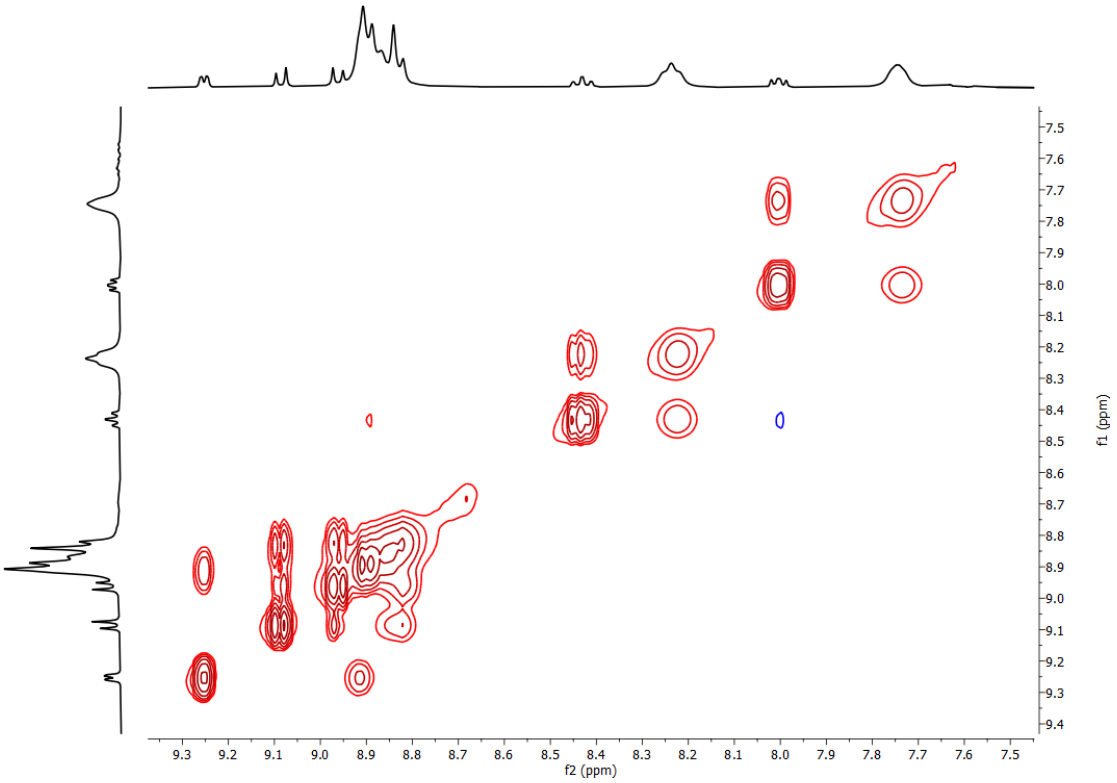

Figure S7: ^{1}H-^{1}H NOESY NMR spectrum (aromatic region) of a mixture of [$Zn_3(\mu_2$-BPNP)(μ_2-OAc)$_3$(OAc)$_2$(μ_3-OH)] (**3**) and [Zn(BPNP)(OAc)$_2$] (**2**) in DMSO-*d*$_6$, indicating that complex **2** and **3** are interchanging.

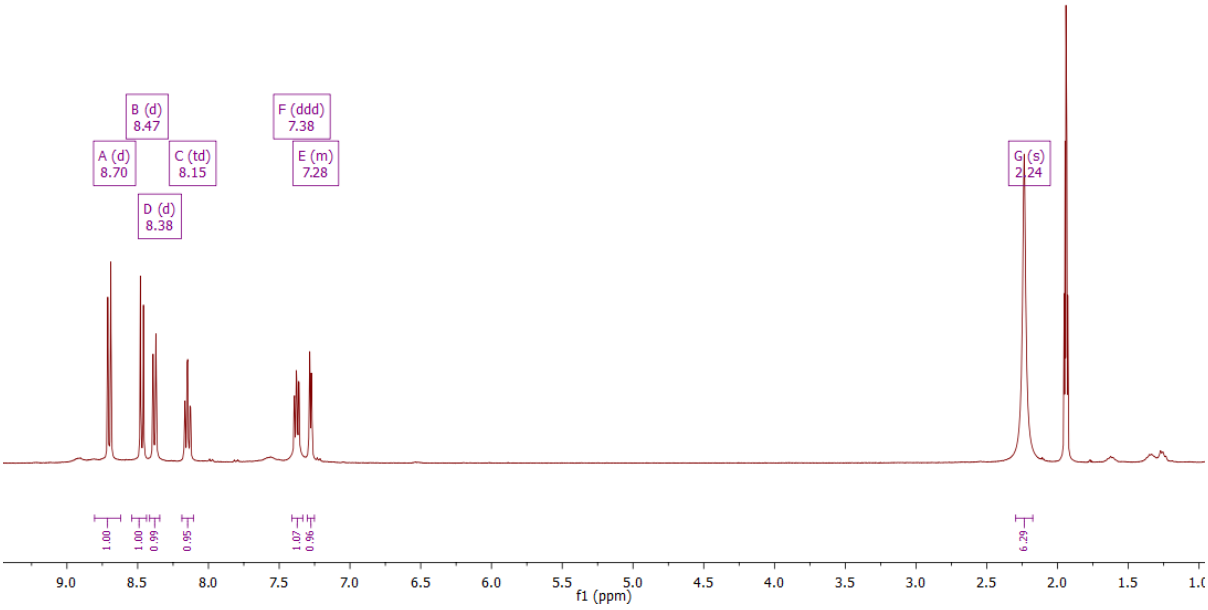

Figure S8: ^{1}H NMR spectrum of the product of BPNP and non-anhydrous Zn(OTf)$_2$ in MeCN-*d*$_3$. The signal at 2.24 ppm is likely due to H_2O bound to the zinc centre.

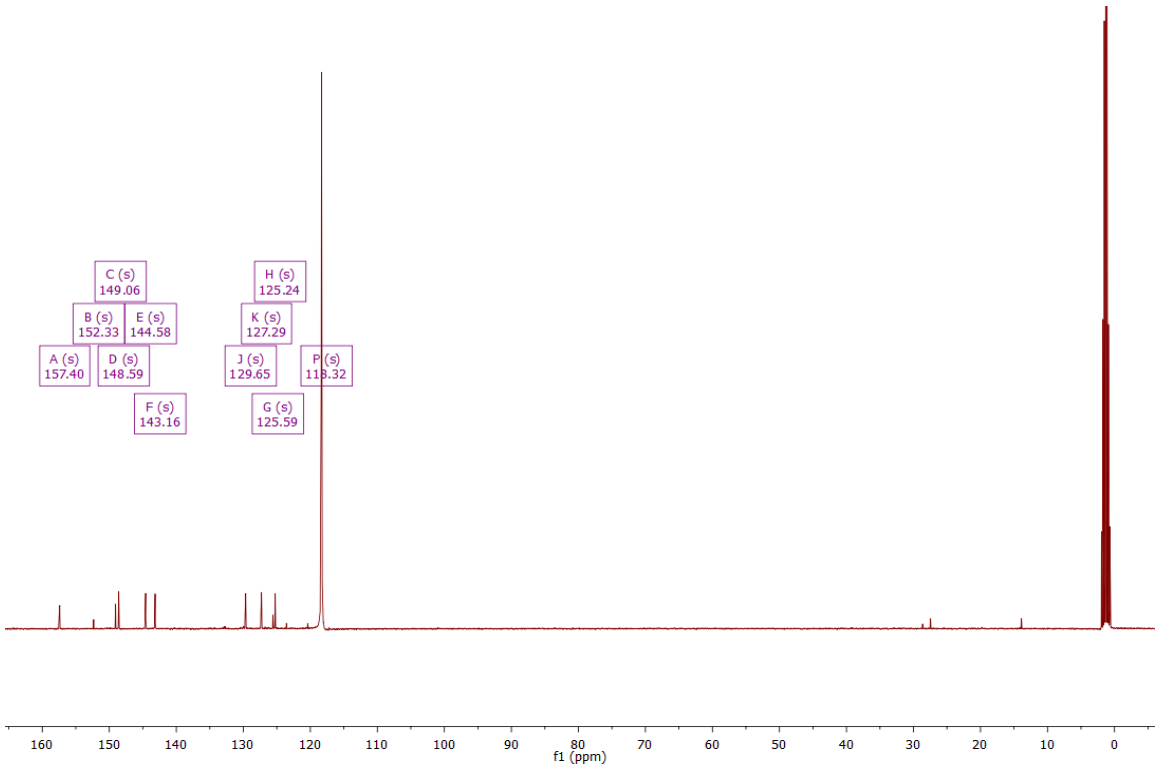

Figure S9: $^{13}C\{^{1}H\}$ NMR spectrum of the product of BPNP and non-anhydrous $Zn(OTf)_2$ in MeCN-d_3.

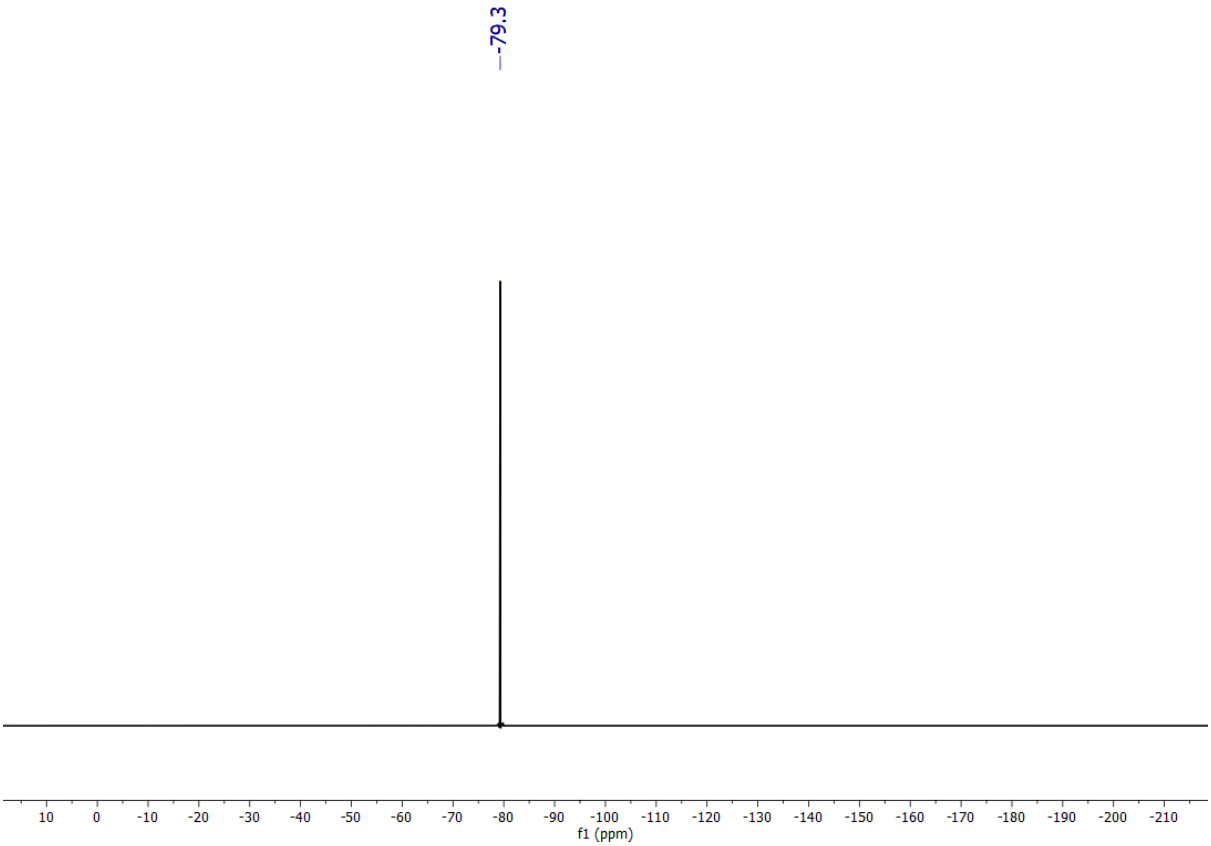

Figure S10: $^{19}F\{^{1}H\}$ NMR spectrum of the product of BPNP and non-anhydrous $Zn(OTf)_2$ in MeCN-d_3.

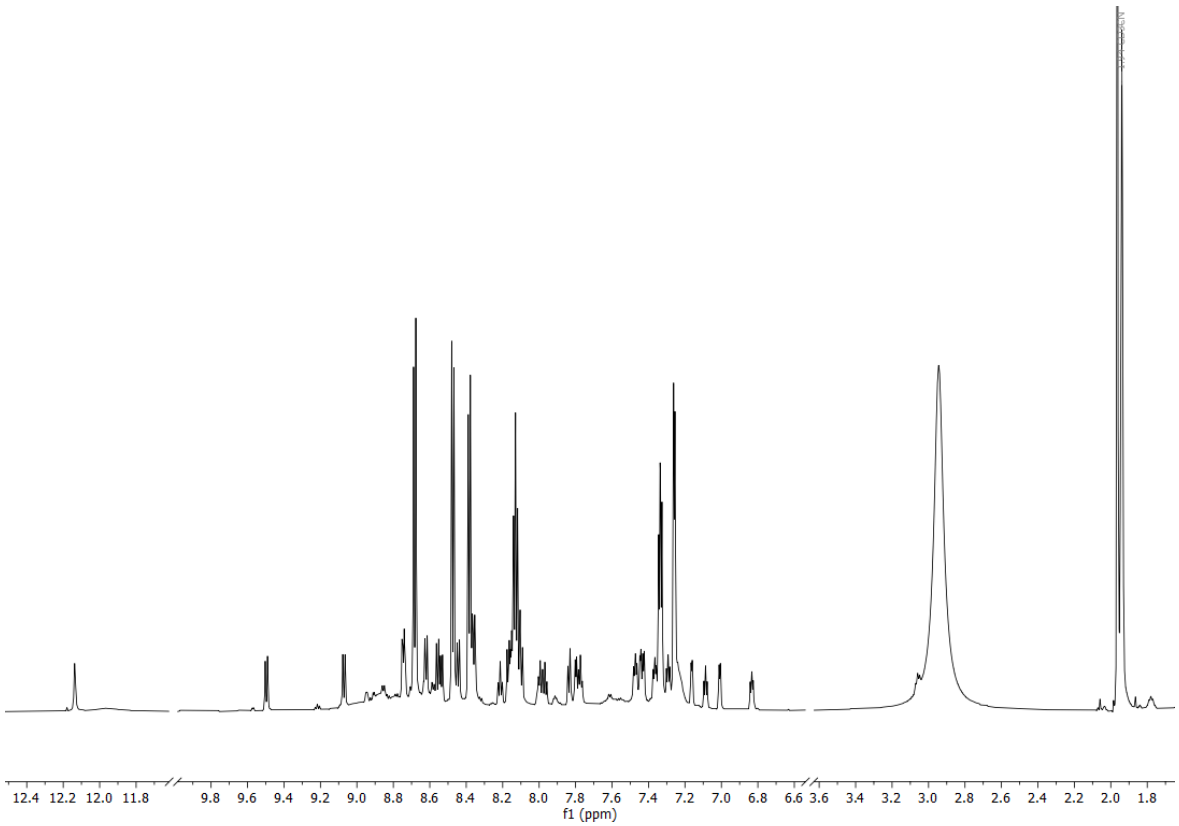

Figure S11: ^{1}H NMR spectrum at −40 °C of the product of BPNP and non-anhydrous $Zn(OTf)_2$ in MeCN-d_3, showing an array of species present.

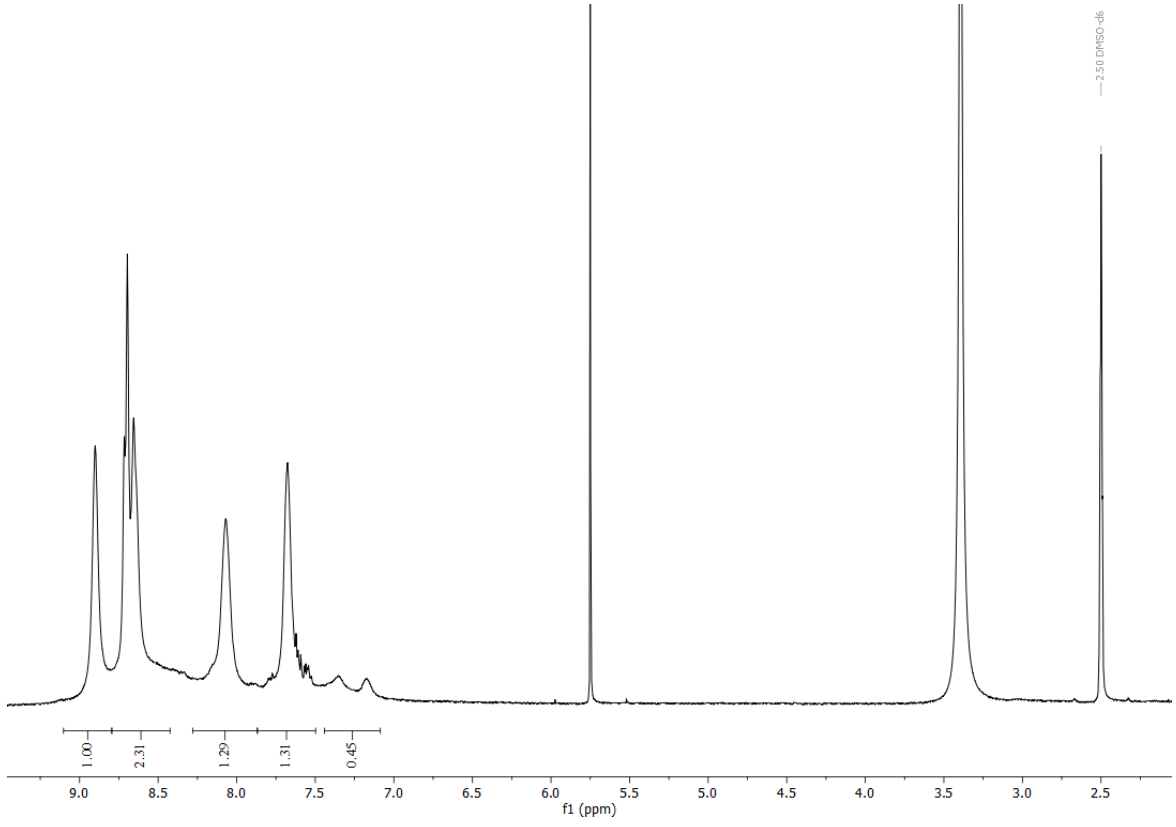

Figure S12: ^{1}H NMR of the product of BPNP and anhydrous $Zn(OTf)_2$ in DMSO-d_6. Some residual DCM from the ligand synthesis is also present.

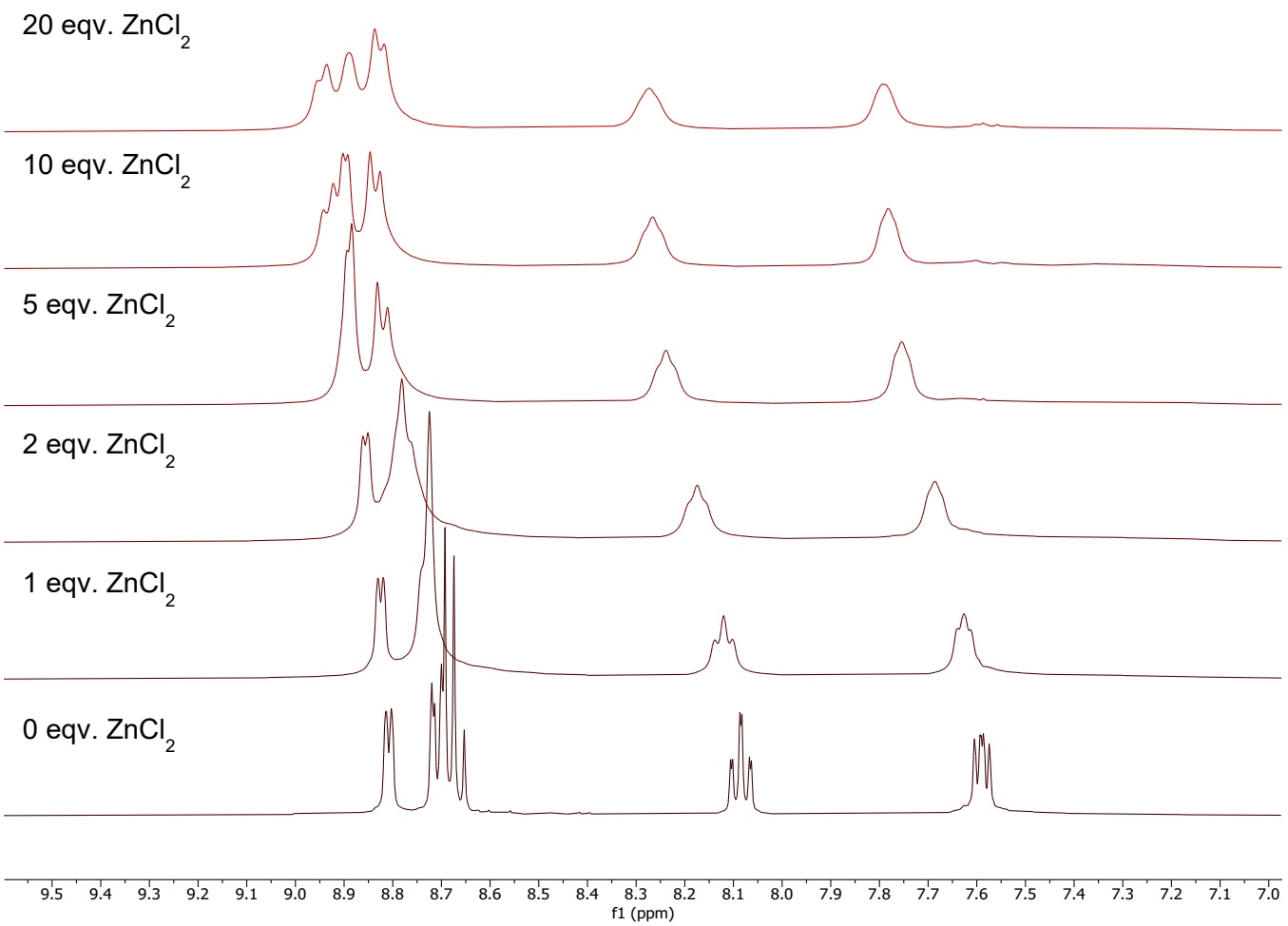

Figure S13: ^{1}H NMR spectra (aromatic region) of the reactions between BPNP and $ZnCl_2$ in DMSO-*d*$_6$ in various stoichiometric ratios.

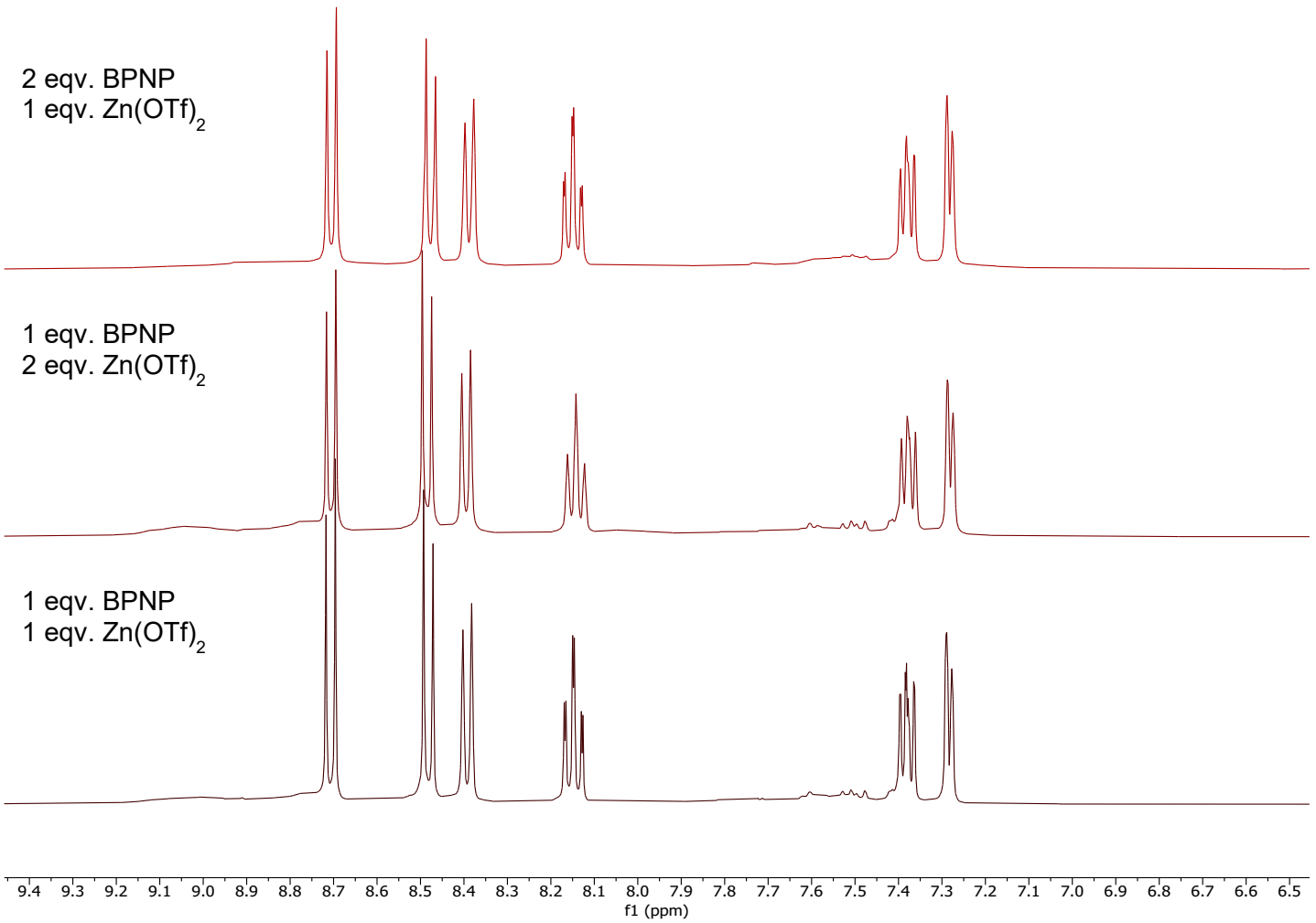

Figure S14: ^{1}H NMR spectra (aromatic region) of the reactions between BPNP and anhydrous $Zn(OTf)_2$ in anhydrous MeCN-d_3 in various stoichiometric ratios.

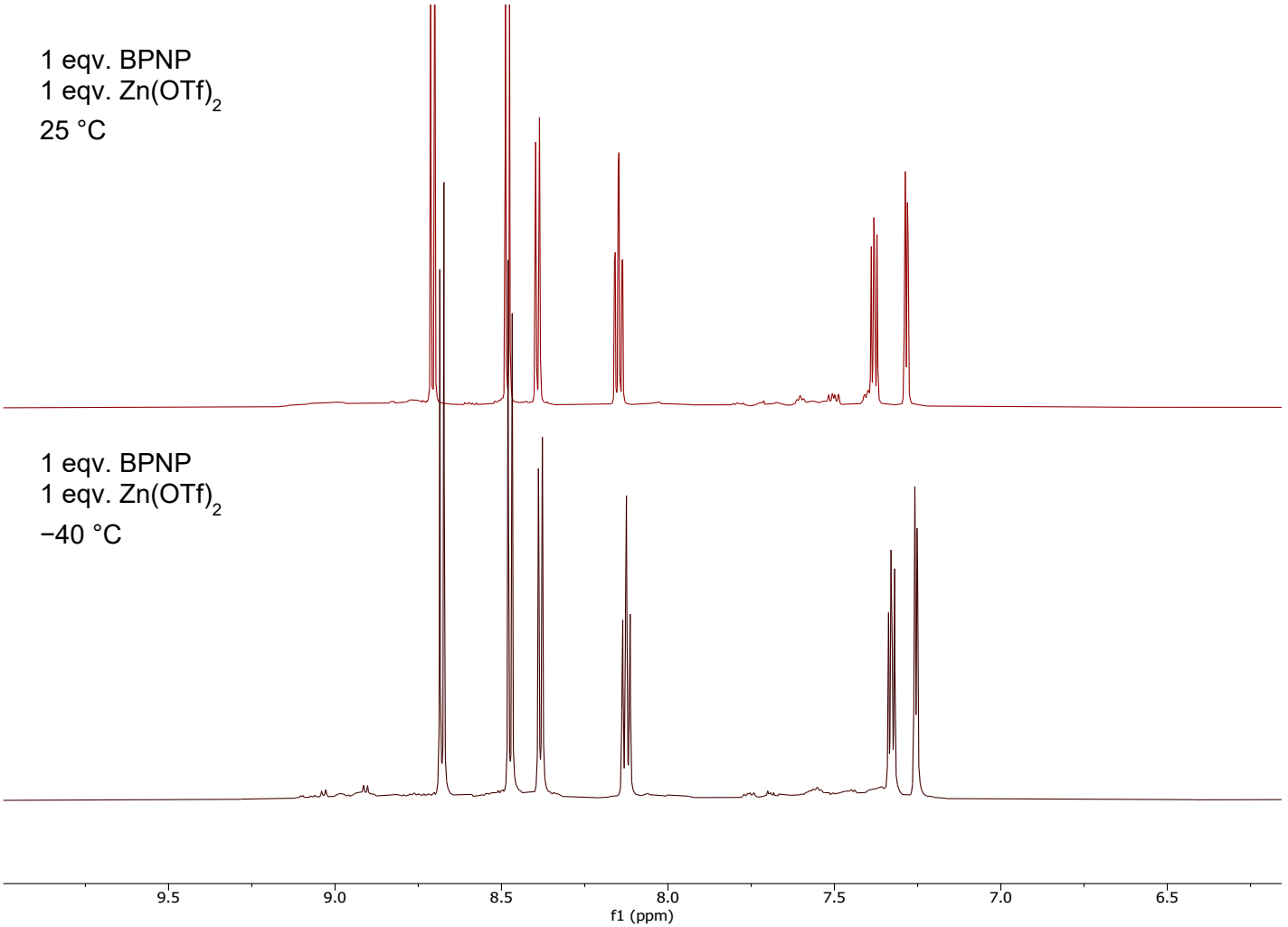

Figure S15: ^{1}H NMR spectra (aromatic region) of the reactions between BPNP and anhydrous $Zn(OTf)_2$ in a 1:1 ratio in anhydrous MeCN-d_3 at 25 °C and −40 °C.

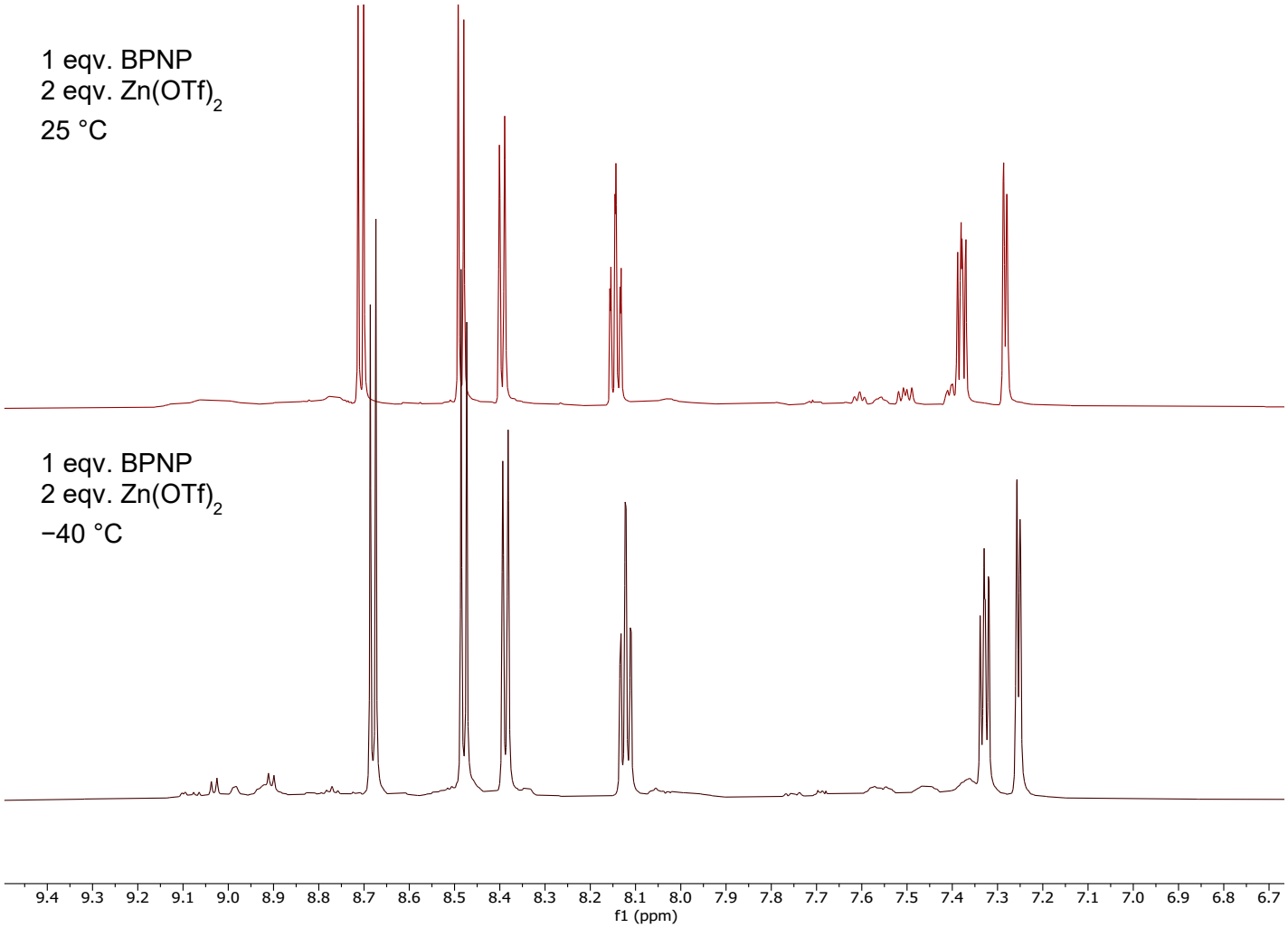

Figure S16: ^{1}H NMR spectra (aromatic region) of the reactions between BPNP and anhydrous $Zn(OTf)_2$ in a 1:2 ratio in anhydrous MeCN-d_3 at 25 °C and −40 °C.

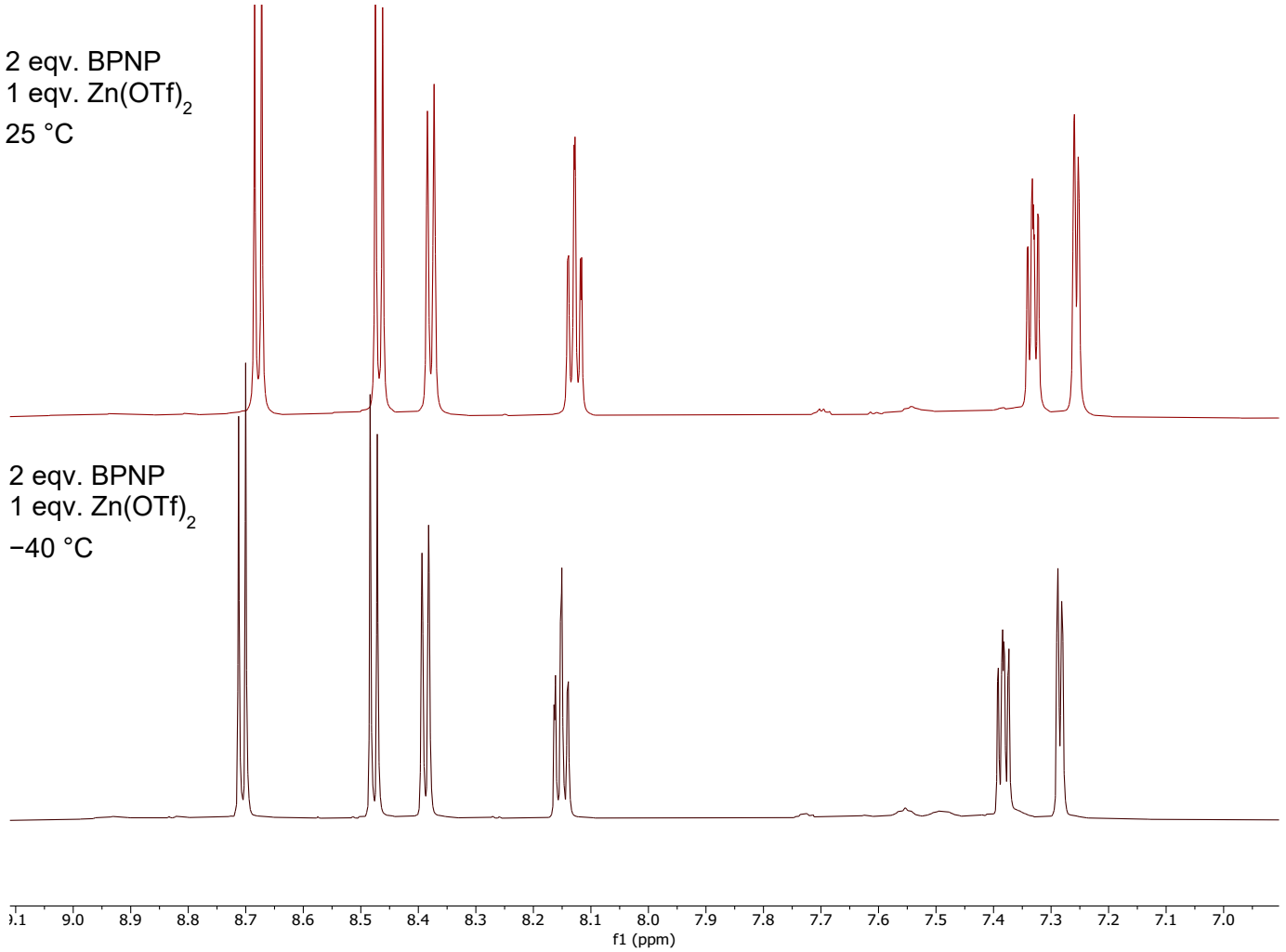

Figure S17: ^{1}H NMR spectra (aromatic region) of the reactions between BPNP and anhydrous $Zn(OTf)_2$ in a 2:1 ratio in anhydrous MeCN-d_3 at 25 °C and −40 °C.

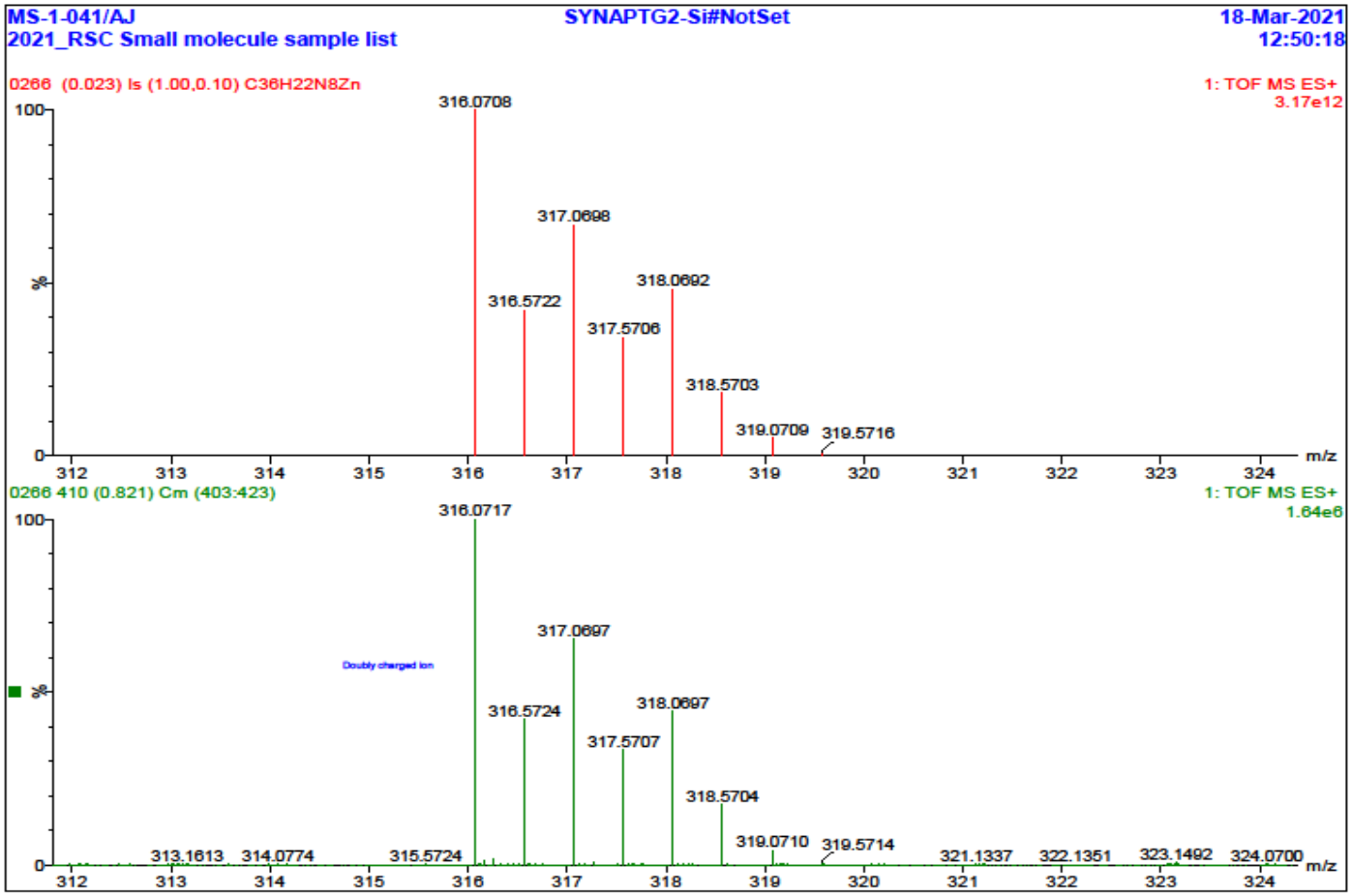

Figure S18: High resolution ESI mass spectrum of the product of BPNP and $Zn(OTf)_2$, showing the doubly charged $[Zn(BPNP)_2]^{2+}$ ion (bottom) compared to calculated (top).

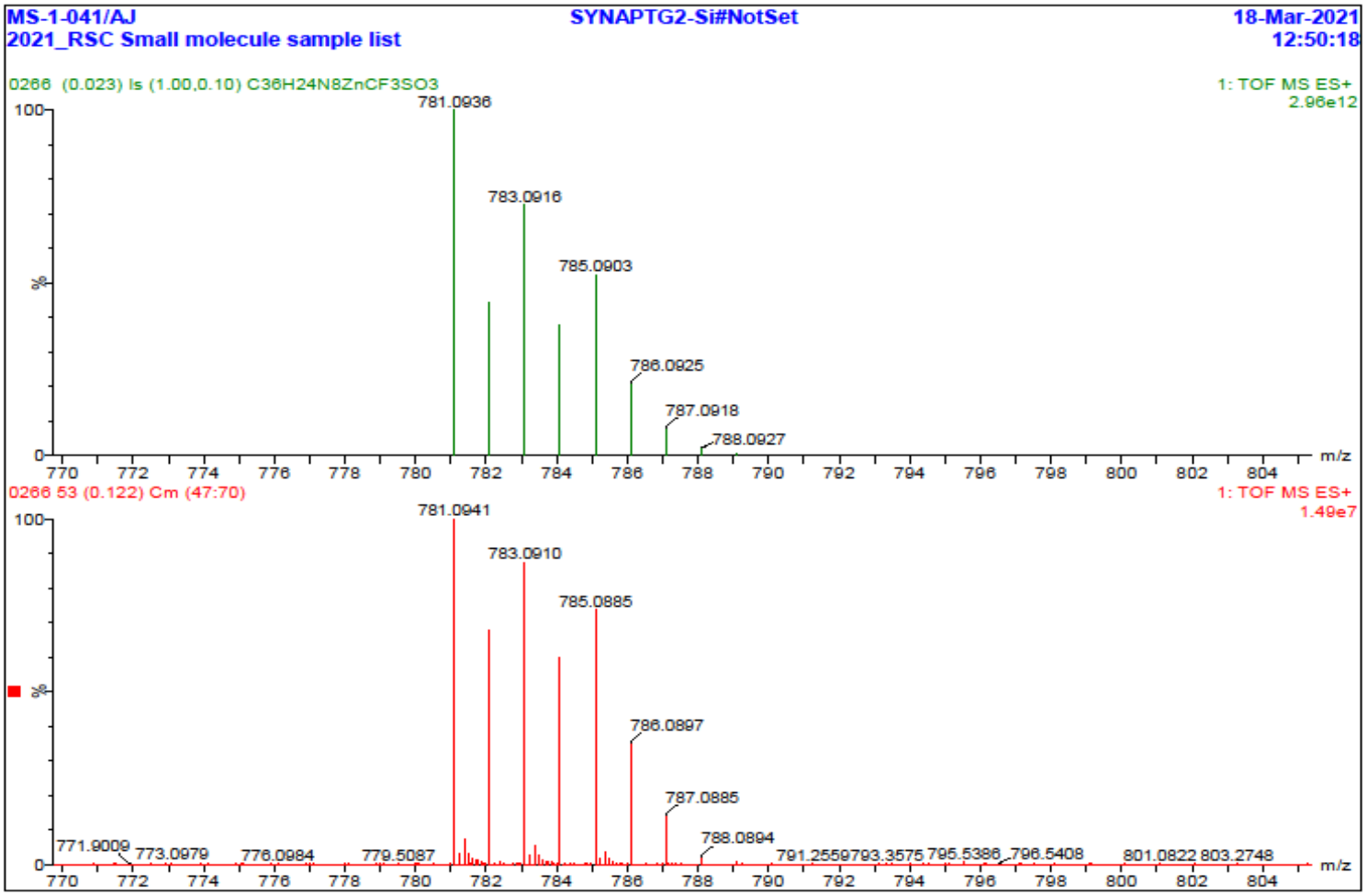

Figure S19: High resolution ESI mass spectrum of the product of BPNP and $Zn(OTf)_2$, showing the complex $[Zn(BPNP)_2](OTf)^{1+}$ ion (bottom) compared to calculated (top).

Table S1: Summary of the crystallographic data

	[Zn(BPNP)Cl_2]. MeCN	[Zn(BPNP)$(OAc)_2$]	[Zn_3(μ^2-BPNP)(μ^2-$OAc)_3(OAc)_2$(μ^3-OH)]. H_2O	[Zn(BPNP-H)$_4$($H_2O)_4$]$(OTf)_3$. $2H_2O$	[Zn(BPNP-H)(NCMe)$(OTf)_2$] (OTf)	[$Zn_2$$(BPNP)_4$($\mu^2$-$H_2O)_2$]$(OTf)_4$. $4H_2O$
CCDC Number	**2070528**	**2070529**	**2070530**	**2070531**	**2070532**	**2076076**
Chemical formula	$C_{20}H_{15}Cl_2N_5Zn$	$C_{22}H_{18}O_4N_4Zn$	$C_{28}H_{28}N_4O_{12}Zn_3$	$C_{21}H_{21}O_{15}N_4ZnF_9S_3$	$C_{23}H_{16}F_9N_5O_9S_3Zn$	$C_{76}H_{56}F_{12}N_{16}O_{18}S_4Zn_2$
Formula mass	461.64	467.77	808.65	906.00	838.96	1968.34
Crystal system	Triclinic	Monoclinic	Monoclinic	triclinic	Triclinic	Triclinic
a/Å	7.3656(4)	11.7191(8)	34.6586(4)	10.5672(5)	9.1173(4)	11.87210(10)
b/Å	9.1837(4)	21.9897(12)	11.49080(10)	13.2605(9)	13.6192(5)	13.95150(10)
c/Å	15.0964(10)	7.9602(6)	15.9771(2)	13.8282(7)	13.9012(5)	24.1101(3)
α/°	98.872(4)	90	90	64.008(6)	106.687(3)	93.6910(10)
β/°	93.682(5)	99.534(7)	103.3090(10)	77.931(4)	103.794(4)	92.3790(10)
γ/°	105.844(4)	90	90	85.995(4)	95.233(3)	93.1380(10)
Volume/$Å^3$	964.53(10)	2023.0(2)	6192.07(12)	1702.69(18)	1581.91(11)	3975.12(7)
Temperature/K	150	150	150	150	150	150
Space group	P**1**	P21/c	C21/c	P1	P1	P1
Z	2	4	8	2	2	2
Radiation type	Cu Kα	Cu Kα	Cu Kα	Cu Kα	Cu Kα	Cu Kα
Absorption coefficient	4.446	2.014	3.326	3.86	3.857	2.694
No of reflections measured	3491	6269	9642	9631	8943	58699
No of independent reflections	2922	3755	5391	3788	5848	15976
R_{int}	NA – twinned data set	6.56	2.05	3.39	0.0309	1.78
Final R1 values (I > 2σ(I))	3.45	7.05	3.64	3.90	0.0399	5.07
Final wR(F2) values (I > 2σ(I))	8.54	19.96	9.84	9.78	0.0998	13.04
Goodness of fit on F^2	0.952	1.049	1.064	1.016	1.038	1.061